Frontiers in Heat and Mass Transfer

Available at www.ThermalFluidsCentral.org

CROSSFLOW AND HEAT TRANSFER CHARACTERISTICS ACROSS A CAM-SHAPED TUBE BANK: A NUMERICAL STUDY

M. O. Petinrin[a], B. A. Sikirullahi[a], T. T. Olugasa[a] and O. M. Oyewola [a,b,*]

[a] Department of Mechanical Engineering, University of Ibadan, Ibadan, Nigeria
[b] School of Mechanical Engineering, Fiji National University, Suva, Fiji

ABSTRACT

Tubes are commonly employed in heat exchangers for their ease of production and capacity to sustain high pressure. In this study, the heat and flow transfer behaviour of cam-shaped tube bank in staggered configuration at varying angles of attack 0° to 180° was numerically investigated. The study was carried out by solving the continuity, momentum, energy and realizable k-ε transport equations using the finite volume-based ANSYS Fluent solver. This was performed to acquire the friction factor and heat transfer characteristics in the air inlet velocity range of 9 to 15 m/s. The results showed that the cam-shaped tube bank at varying angles of attack provided enhanced heat transfer characteristics relative to the circular tube bank. Also, cam-shaped tube banks at angles of attack of 90° and 120° exhibited the maximum heat transfer with 33.9 and 32.1% increase in Nusselt number over the circular tubes. Their friction factor was higher by 183 and 140.7%, respectively. The cam-shaped tube banks generally exhibited higher performance than the circular tube bank. Tube banks at angles of attack of 150° and 180° demonstrated higher thermal-hydraulic performance by 167.6 and 284.3% than the circular tubes, respectively. However, the tube banks at angles 90° and 120° exhibited lesser performance by value of 52.6 and 45.1%.

Keywords: *heat exchanger; cam-shaped tube bank, thermal-hydraulic performance, angle of attack, numerical analysis*

1. INTRODUCTION

In a variety of industrial engineering applications, forced convective flow over tube banks is widely used. More specifically, they are used to make more compact heat exchangers with better heat transfer performance (Ahmed et al., 2017; Nouri-Borujerdi & Lavasani, 2007). Some of the applications of these tubes in heat exchangers are found in cooling towers, oil and gas industries, waste heat recovery, solar air-water heater, chemical processing unit, pharmaceutical industries, cogeneration, HVAC, automotive radiators and so on (Bayat et al., 2014; Mangrulkar et al., 2016). The continued interest in the utilization of highly efficient thermal components and subsystems with less energy demand has led researchers in the last few decades to many alternative designs of tube banks for heat exchanger applications (Mangrulkar et al., 2016).

Several studies had been carried out on enhancing the thermal interaction between tubes and the working fluids, which are either by active or passive means. Enhancement carried out using the active mode entails changing fluid flow properties such as flow turbulence by swirl generators or secondary fans, surface vibration, and thermal conductivity of the working fluid. The passive enhancement technique involves modification of the flow geometry's surface, tube cross-section, pitch ratio, orientation of tubes or tube arrangement in order to enhance the heat transfer rate. Nevertheless, the choice of any of the two techniques also alters the friction characteristics of a system (Mangrulkar et al., 2019).

Huang and Jang (2012) used a computational model to investigate staggered and in-line tube banks during laminar forced convection of a water-based Al_2O_3 nano - fluids suspension. It was found that the staggered array of tubes exhibited higher heat transfer and pressure drop when compared to inline array of tubes. Khan et al. (2006) conducted an investigative study of heat energy transfer in flow channel for a tube

bundle using the integral method and discovered that the more compact the tube banks were, the higher the heat transfer rates recorded, and that the staggered configuration had improved heat transfer output than the inline configuration. Ahmed et al. (2017) numerically investigated laminar convective flow of Al_2O_3-water nanofluid flow over staggered circular-tube banks in isothermal wall condition. In the Reynolds number ranges evaluated, they had the highest performance at 1.5 longitudinal pitch ratio, 2.5 transverse pitch ratio, and 5% nanoparticle volume fraction. Petinrin et al. (2019) studied the thermal and friction characteristics of flow over staggered circular tube banks with varying tube pitches numerically. It was found that the tube bundles with decreasing pitches performed better in terms of heat transfer, whereas those with increasing pitches had a reduced friction factor. To improve the thermal and hydraulic performance, Ge et al. (2021) performed a CFD study and multi-objective optimization of shape design for a tube bank in turbulent flow. Twenty-five polar radii and five tubes with various forms were taken into consideration. Their findings indicated that the tube bank with the best tube shapes gave a boost on heat transfer by 7.6% while maintaining the same pressure drop. Xiao & Zhang (2022) performed a 3D simulation to calculate the heat transfer, friction factor and exergy loss related to flow across three different arrangements of tubes in the Reynolds number range of 13,000 to 20,000. Their results showed that the arrangement significantly affects the thermal and hydrodynamic performances of the tube banks, with the staggered arrangement of tubes outperforming the in-line arrangement.

Circular tubes are often used in heat exchangers because they are simple to manufacture and can withstand high pressure. However, due to separation in the boundary layer when fluid flows across circular tubes, huge separation zones are created at the tube's rear end, which result in severe vibrations, large pressure drops and even tube collapse (Guanmin et al., 2015; Nouri-Borujerdi & Lavasani, 2007). These have caused a shift of focus by many researchers more on the non-circular tube

* Corresponding author. Email: oooyewola001@gmail.com

sections leading to their prominence in industrial applications (Nada et al., 2007). In recent years, more streamlined, very low hydraulic resistance cross-sections have been investigated such as the elliptic, flat, oval and cam-shaped tubes as heat transfer media in cross flow heat exchangers (Bayat et al., 2014; Nouri-Borujerdi & Lavasani, 2007).

Toolthaisong & Kasayapanand (2015) experimentally studied the effect of angles of attack on non-fin cross-flow heat exchanger with flat tube arrays in staggered arrangement. They found that the change in airflow angles of attack had significant implications on the thermal and flow characteristics of the tubes. In heat exchanger implementations, Bahaidarah et al. (2005) explored constant laminar two-dimensional incompressible flow over both in-line and staggered flat tube banks. It was indicated from their study that circular tubes of equivalent diameter performed better thermal characteristics than flat tube banks but with higher pressure drop. Han et al. (2013) conducted numerical research on both circular and oval tubes with increased fins, wavy fins, and louvered fins, and found that all of the tube bank designs had higher thermal efficiency than their circular tube counterparts.

Guan-min et al. (2015) investigated the heat and flow transfer properties of egg-shaped tubes made from a semicircle (upstream) and a semi-ellipse (downstream) with axis ratios ranging from 1 to 5, with 1 being a circular tube. The egg-shaped tubes with a value of 2 were found to have excellent performance indicator. Laminar flow across a fin and flat tube heat exchanger with different aspect ratios was examined numerically by Alnakeeb et al. (2021). The results indicated that the pressure drop and heat transfer per unit of fan power are significantly influenced by the flat-tube aspect ratio. It was observed that when the flat tube aspect ratio decreased from 1 (circular tube) to 0.33, the pressure drop decreased by 33.7% and 57.3%, with an air inlet velocity of 0.5 and 3.5 m/s, respectively. Deeb (2021) conducted a study using both experimental and numerical methods on the impact of angle of attack on fluid flow parameters around a single drop-shaped tube. They discovered that the drop-shaped tubes delay the boundary layer's separation from the tube wall and also demonstrated their superiority over circular tubes in terms of decreased drag and friction factor under the same operating conditions. Deeb (2022) further carried out an investigation on heat transfer and fluid flow across bundles of staggered drop-shaped tubes with different longitudinal and transverse pitch ratios. According to their findings, an increase in transverse pitch has a greater impact on heat transfer than an increase in longitudinal pitch. Finally, they asserted that under the same operating conditions, the bundle of drop-shaped tubes outperformed the circular ones in terms of high thermal-hydraulic performance.

The flow and heat transfer across an inline arrangement of mixed tube bundles made up of circular and cam-shaped tubes with the same circumferential lengths was experimentally studied by Abolfathi et al. (2021). They found that cam-shaped tubes in mixed bundles had higher thermal-hydraulic performance than the circular tubes. Lavasani & Bayat (2016) used numerical simulations to investigate the heat and flow transmission of nanofluid via cam-shaped and circular tubes with staggered and in-line arrangements. The cam-shaped tube bank performed better in terms of friction and heat transfer, according to their findings. Mangrulkar et al. (2016) discovered that the ratio of heat transmission to friction factor of the inline cam-shaped tube bank was roughly 5 times greater than that of the circular tubes in another simulation analysis. Bayat et al. (2014) found that the heat transfer efficiency of cam-shaped tube banks in staggered configuration was about 6 times that of circular tube banks in similar system. Mangrulkar et al. (2018) investigated the thermal performance of crossflow across cam-shaped tubes using a numerical analysis. Their study revealed that the thermal-friction factor ratio of the cam-shaped tubes was significantly better than that of the circular tubes.

As a result of earlier investigations, it is obvious that cam-shaped tube banks outperform traditional circular tube banks in terms of thermal and hydraulic performance. Studies have also established that angles of attack have pronounced effect on the thermal and flow characteristics of tube banks, but there has been dearth of literatures on cam-shaped tube

banks at varying angles of attack. The few reported cases were of single cam-shaped tubes or cylinders (Lavasani, 2011; Nouri-Borujerdi & Lavasani, 2007, 2008). Hence, the focus of this research will be on numerical analysis of the hydraulic and thermal characteristics of cam-shaped tube banks in staggered configuration under various angles of attack. This investigation is carried out to examine the influence of angles of attack of flow of the cam tubes on thermal-hydraulic performance.

2. METHODOLOGY

The numerical study was carried out employing the computational fluid dynamics software, ANSYS. The equations governing the temperature, velocity and pressure fields were discretized and solved using the finite volume software code ANSYS Fluent 18.1. The ANSYS CFD Post and MS Excel were used in presenting the results of the simulations in graphical forms.
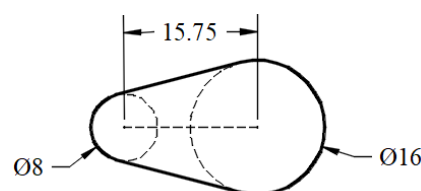
2.1 Geometry of the tube bundles

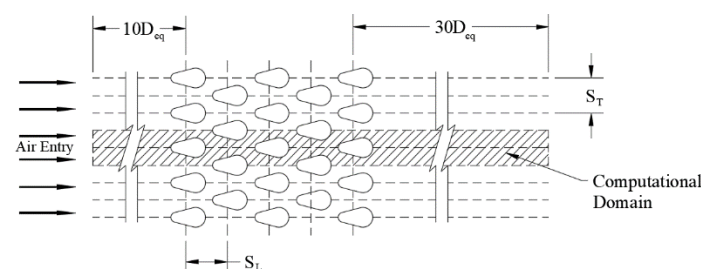**Fig. 1.** The cam-shaped tube cross-section

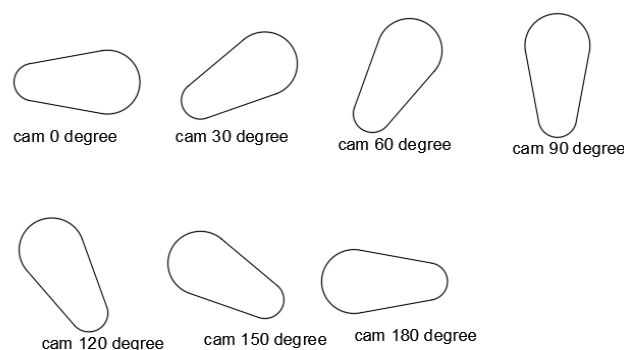**Fig. 2.** The cam-shaped tube bank in staggered arrangement

Fig. 3. The cam-shaped tubes at varying angles of attack to the flow direction

The geometry considered is a cam profile which is compared with a circular tube of equivalent diameter. The cam-shaped tube geometry, which is identical in size to Bayat et al. (2014) experimental investigation, consists of two circles of various diameters joined by two tangential lines (Fig. 1). The diameters of the circles are $d = 8$ mm and $D = 16$ mm, having a distance, l of 15.75 mm between their centers. The characteristic length of the tube cross-section was evaluated as the diameter of an equivalent cylinder, $D_{eq} = 22.35$ mm using (Khurmi & Gupta, 2005):

$$D_{eq} = \frac{(D+d)}{2} + 2l + \frac{(D-d)^2}{4l} \qquad (1)$$

Figure 2 shows the solution domain of the cam-shaped tube bank investigated in the study. The transverse pitch ratio, S_T/D_{eq}, was kept at 1.255 in this investigation, while the longitudinal pitch ratio, S_L/D_{eq}, was kept at 1.506. The downstream and upstream lengths are maintained at $10D_{eq}$ and $30D_{eq}$, respectively, to create a stable flow at the entrance and exit zones. The experiment was then repeated for cam tubes with attack angles of 0°, 30°, 60°, 90°, 120°, 150°, and 180° to the flow direction (Fig. 3).

2.2 Mesh Generation

The computational domain has a collection of tube rows within a test section. The automatic method was specified to obtain a mesh with high quality throughout the entire domain. Also, the domain was body sized, and an inflation with 10 layers was created on all the tube edges. A mesh quality of not less than 0.61 was maintained for each of the cross-sections of the angles of attack. The fluid domain was meshed using quadrilateral mesh elements. For all the angles of attack a range of 55512 – 59382 number of elements was attained. The illustration of the structured mesh over the domain is shown in Fig. 4.
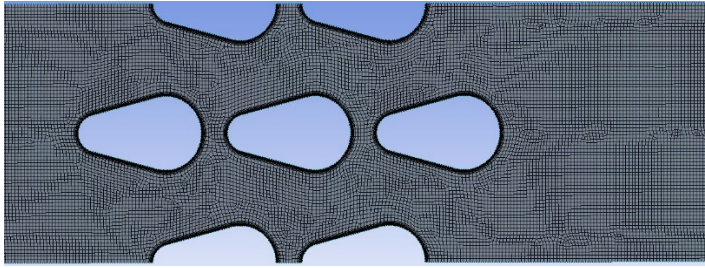

Fig. 4. Structured mesh around the tube surface

2.3 Model Selection

The model selection was guided by first by determining the range of Reynold's number that characterize the flow regime, which was calculated from the expression;

$$Re = \frac{\rho U_{max} D_{eq}}{\mu} \qquad (2)$$

where Re is the Reynold's number, ρ is the density of the fluid, U_{max} is the maximum velocity in the narrow section of the circular tubes, D_{eq} is the equivalent diameter and μ is the dynamic viscosity.

The Realizable k-ε model was used with non-equilibrium wall functions because it fulfills some theoretical limitations on Reynold stresses and is consistent with the physics of fluid motion (Shih et al., 1995). The equations for momentum conservation, continuity and conservation of energy are presented below.

Equation of continuity; $\dfrac{\partial u_i}{\partial x_j} = 0 \qquad (3)$

Conservation of momentum equation;

$$\rho \frac{\partial (u_j u_i)}{\partial x_j} = -\frac{\partial P}{\partial x_i} + \frac{\partial}{\partial x_j} \left[(\mu + \mu_T) \left(\frac{\partial u_i}{\partial x_j} + \frac{\partial u_j}{\partial x_i} \right) + \frac{2}{3} \rho k \delta_{ij} \right] \qquad (4)$$

Energy equation;

$$\rho c_p \frac{\partial (u_j T)}{\partial x_j} = \frac{\partial}{\partial x_j} \left((\lambda + \lambda_T) \frac{\partial T}{\partial x_j} \right) \qquad (5)$$

given that

$$\lambda_T = \frac{\mu_T c_p}{Pr_T} \qquad (6)$$

where x_i (i = 1, 2) is the coordinates, u_i represents the velocity vector, P is the pressure, T represents temperature, ρ is the density, μ is the dynamic viscosity, μ_T is the turbulent eddy viscosity, λ stands for the thermal conductivity, λ_T stands for turbulent thermal conductivity, c_p stands for the specific heat capacity, Pr_T is the turbulent Prandtl number.

The turbulence eddy viscosity as obtained from Shih et al. (1995);

$$\mu_T = \rho C_\mu \frac{k^2}{\varepsilon} \qquad (7)$$

From equation (7)

$$C_\mu = \frac{1}{A_o + A_s \dfrac{kU^*}{\varepsilon}} \qquad (8)$$

And

$$U^* = \sqrt{S_{ij}S_{ij} + \bar{\Omega}_{ij}\bar{\Omega}_{ij}} \qquad (9)$$

also

$$\bar{\Omega}_{ij} = \Omega_{ij} - 2\varepsilon_{ijk}\omega_k$$

$$\Omega_{ij} = \bar{\Omega}_{ij} - \varepsilon_{ijk}\omega_k$$

where $\bar{\Omega}_{ij}$ is the mean rate of rotation tensor viewed in a moving reference frame with angular velocity ω_k.

Thus, the model constants A_o and A_s are given, respectively as

$$A_o = 4.04 \text{ and } A_s = \sqrt{6} \cos \psi$$

also given that

$$\psi = \frac{1}{3} \cos^{-1} \left(\sqrt{6}W \right), \; W = \frac{S_{ij}S_{jk}S_{ki}}{\tilde{S}^3}, \; \tilde{S} = \sqrt{S_{ij}S_{ij}} \;,$$

$$S_{ij} = \frac{1}{2} \left(\frac{\partial u_i}{\partial x_j} + \frac{\partial u_j}{\partial x_i} \right)$$

The additional transport equations for the realizable k-epsilon model is given by;
Turbulent kinetic energy:

$$\rho \frac{\partial (u_j k)}{\partial x_j} = \frac{\partial}{\partial x_j} \left[\left(\mu + \frac{\mu_T}{\sigma_k} \right) \frac{\partial k}{\partial x_j} \right] + \left[\mu_T \left(\frac{\partial u_i}{\partial x_j} + \frac{\partial u_j}{\partial x_i} \right) - \frac{2}{3} \rho k \delta_{ij} \right] \frac{\partial u_i}{\partial x_j} - \rho \varepsilon \qquad (10)$$

Turbulent dissipation energy:

$$\rho \frac{\partial (u_j \varepsilon)}{\partial x_j} = \frac{\partial}{\partial x_j} \left[\left(\mu + \frac{\mu_T}{\sigma_\varepsilon} \right) \frac{\partial \varepsilon}{\partial x_j} \right] + \rho C_1 S_\varepsilon - \rho C_2 \frac{\varepsilon}{k + \sqrt{\upsilon\varepsilon}} \qquad (11)$$

Other parameters are;

$$C_1 = \max \left[0.43, \frac{\eta}{\eta + 5} \right], \text{ and model constants;}$$

$$C_{\varepsilon 1} = 1.44, C_2 = 1.9, \sigma_k = 1.0, \sigma_\varepsilon = 1.2$$

where $\eta = S \dfrac{k}{\varepsilon}$, $S = \sqrt{2 S_{ij} S_{ij}}$

2.4 Boundary conditions and Numerical Scheme

The velocity of the working fluid – air was initialised as zero while the pressure and temperature were taken to be at zero-gauge pressure and 303.15 K, respectively. Velocity conditions were specified at the inlet of the computational domain by varying the velocity from 9 m/s to 15 m/s, and also the inlet temperature was maintained at 303.15 K. At the outlet boundary, zero gradients were set for velocity and temperature while zero-gauge was imposed for pressure. Fixed temperature of 353.15 K and wall functions were applied at the walls of the tubes. The energy and momentum governing equations were discretized using the second-order upwind approach. The pressure-based continuity, momentum and two k-ε model equations were solved jointly using the pressure-based coupled solver. For the energy and continuity equations, the scale residual convergence conditions were on the order of 10^{-6}. For initializing the temperature and velocity fields in the computational domain, the hybrid initialization method was used.

2.5 Data Reduction

It is important to obtain the flow and thermal field parameters in order to estimate the friction factor, Nusselt numbers, and thermal-hydraulic performance. The heat loss to the surroundings was assumed to be negligible. Therefore, the heat transfer from the walls of the tube banks to the air-stream is given by (Bergman et al., 2011);

$$Q = hA\Delta T_{LM} \tag{12}$$

where the log mean temperature difference is,

$$\Delta T_{LM} = \frac{\left(T_w - T_{in}\right) - \left(T_w - T_{out}\right)}{\ln \dfrac{\left(T_w - T_{in}\right)}{\left(T_w - T_{out}\right)}} \tag{13}$$

and the surface area was calculated from,

$$A = \pi d_o L n \tag{14}$$

Hence, in order to derive the coefficient of heat transfer, the rate of heat transfer from equation (14) was derived from the heat accompanying the temperature difference within the air stream as;

$$Q = \dot{m} c_p \left(T_{out} - T_{in}\right) \tag{15}$$

The average Nusselt is calculated from

$$Nu = \frac{h D_{eq}}{k} \tag{16}$$

where h is the heat transfer coefficient, k is the thermal conductivity property of air obtained at the bulk temperature, $T_{av} = \dfrac{T_{in} + T_{out}}{2}$

For staggered tube arrangement such that $2(S_D - D_{eq}) > (S_T - D_{eq})$, the expression for calculating the maximum velocity is given by (Bergman et al., 2011)

$$U_{max} = \frac{S_T U_\infty}{(S_T - D_{eq})} \tag{17}$$

where S_T and S_D are the transverse pitch and the diagonal pitch, respectively.

The friction factor is estimated from the pressure drop, Δp across tubes as (Holman, 2010).

$$f = \frac{\Delta p}{2\rho v_{max}^2 N} \left(\frac{\mu}{\mu_w}\right)^{0.14} \tag{18}$$

where N is the resistance of the flow.

The thermal-hydraulic performance of the cam-shaped banks is determined in comparison to a circular tube bank of equivalent diameter at the same Reynolds number as (Lavasani et al., 2014).

$$\eta = \frac{(Nu \, / \, f)_{cam}}{(Nu \, / \, f)_{circ}} \tag{19}$$

2.6 Grid Independence Study

The main objective of the mesh-independence analysis was to look for a mesh independent solution. The study was conducted for mesh elements in the range of 23,538 to 57,476. As it can be shown from Fig. 5, the heat transfer coefficient, h becomes independent from the mesh as it approached 57,476 mesh elements. The difference in the heat transfer coefficient between the cases with 45,727 and 57,476 elements is less than 3%. Consequently, to save processing costs, a grid of 57,476 mesh elements was utilised for the simulation.
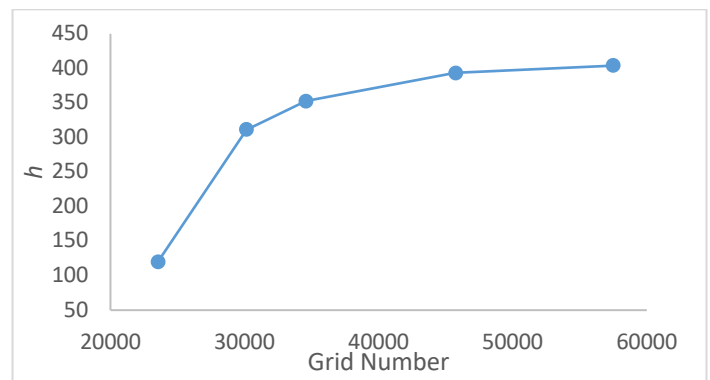

Fig. 5: Grid independence analysis

2.7 Validation of the Model

The Nusselt number values obtained for the circular tube bundle in the present study was compared with the existing analytical correlations, as described in Fig 6. The Zukauskas correlation represents the higher values of Nusselt number, comparing it with numerical study. Though, marginal variation exists for the Nusselt number obtained from the present study, the observed discrepancies may be as a result of the model simplification arising from the constraints placed by the computational cost.
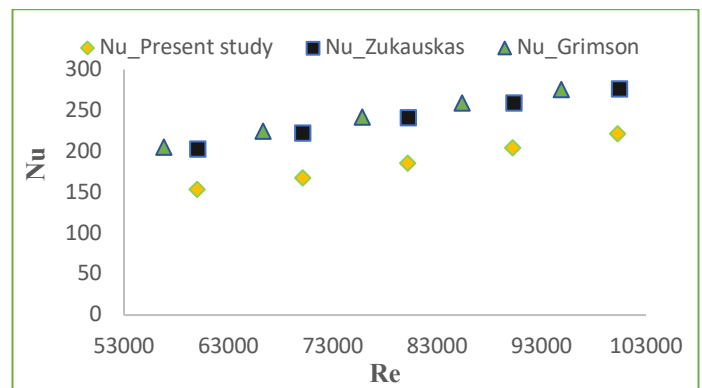

Fig. 6. Comparison of results obtained for the circular tube bank with existing correlations

3.   RESULTS AND DISCUSSION

3.1   Velocity Streamlines

The distributions of airflow velocity across some of the tube banks at inlet velocity 9 m/s are as indicated in Fig. 7. From this figure, both the circular and cam-shaped tube banks exhibit maximum velocity in between the tube walls. Wakes of similar structure developed behind each of the tubes indicate low velocity at these regions. Wakes behind the first four columns are smaller as compared with the fifth column, and this is as a result of delay in flow separation and change in flow structure caused by the tube columns behind the first four columns. Thus, heat transfer is usually at minimum at the wake regions.
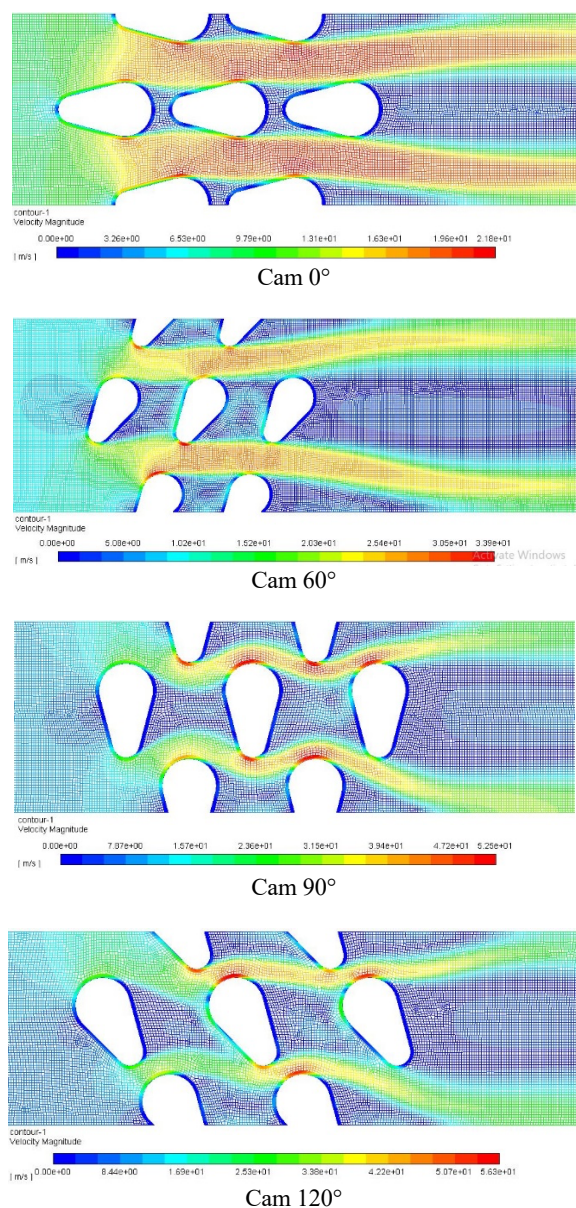

Cam 0°

Cam 60°

Cam 90°

Cam 120°

Fig. 7. Velocity distribution for the circular and cam-shaped tube banks at inlet velocity 9 m/s.

3.2   Effect of changing angles of attack on the air pressure drop

Comparison of the pressure drop across the tube banks at different angles of attack and the circular tube bank are shown in Fig. 8. The maximum and minimum air pressure drops occurred at angles of attack of 90° and 180°, respectively. For the range of airflow velocities, the pressure drop
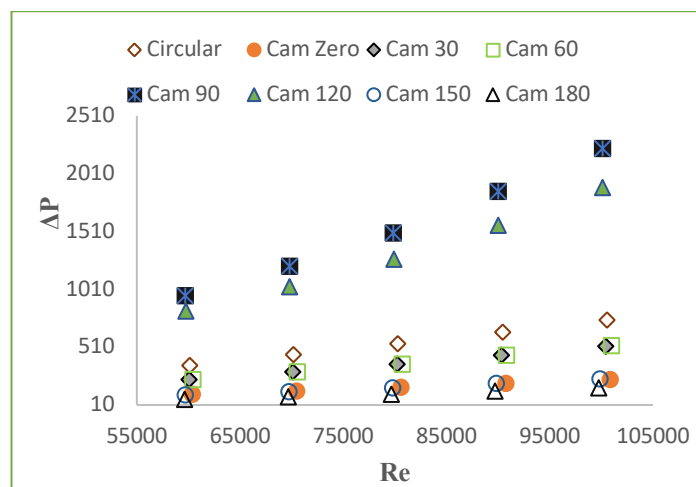

Fig. 8. Pressure drop of the circular and cam-shaped tubes at different angles of attack

Cam 0°

Cam 60°
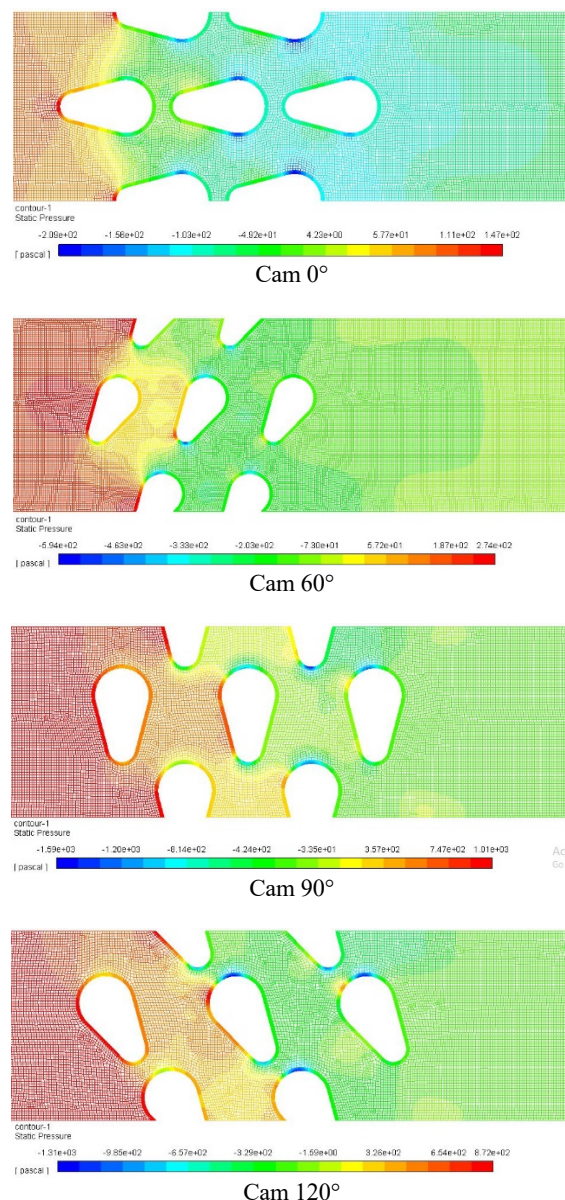

Cam 90°

Cam 120°

Fig. 9. Pressure contour for the circular and cam-shaped tube banks at inlet velocity 9 m/s.

increases with increasing the angles of attack from 0° to 90°, however there is decrease in the pressure drop due to increase in the angles of attack from 90° to 150°.

The circular tube bank depicts higher pressure drop than the cam-shaped tube bank at angles of attack 0°, 30°, 60°, 150° and 180° by about 70.8, 32.5, 33.5, 182.1, 154.4, 71.4, and 80.6%, respectively. However, the cam-shaped tubes with the angles of attack 90° and 120° had increase in pressure drop with of 182.1 and 154. 4% than the circular tube bank, respectively. These indicate that the change in angles of attack of cam-shaped tube banks have noticeable effects on the pressure drop. Also, it was observed generally that increase in velocity of air across the cam-shaped tube banks and circular tube bank results in increase in pressure drop. Fig. 9 shows the pressure distribution for the cam-shaped tubes at varying angles of attack at the inlet velocity 9 m/s.

3.3 The friction factor of airflow across cam-shaped tube banks

Fig. 10 shows the friction factor of airflow over circular tubes and the cam-shaped tubes for all the angles of attack at varying Reynolds numbers. The variation in the friction factors of airflow over the cam tubes at those angles of attack is similar to that of the pressure drops previously described. There was observed decrease in the friction factor as the Reynolds number increases from 55000 to 105000 for all the tube banks. For the cam-shaped tube banks, increase in angles of attack from 0° to 90° results in increase in the friction factor, however there was decrease in the friction factor value due to decrease in the angle of attack from 90° to 150°. These indicate that the tube surface is directly impacted by the air flow, which results in increasing the friction factor than when the air flows across the tube surface tangentially.

The circular tube bank depicts higher friction factor value than the cam-shaped tube bank at angles of attack 0°, 30°, 60°, 150° and 180° by about 70.8, 32.4, 33.7,71.3, and 80.5% respectively. However, the cam-shaped tubes with the angles of attack 90° and 120° have about 183 and 140.7% increase in friction factor values as compared with circular tube bank. These observations indicate that changing angles of attack of the cam-shaped tube banks have noticeable effects on the friction factor.
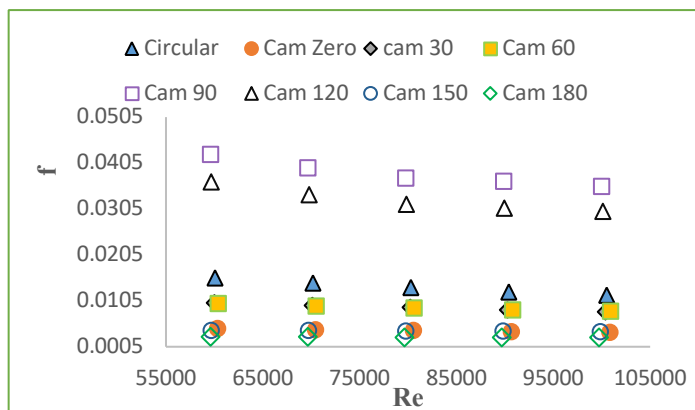

Fig. 10. Friction factor of the circular and cam-shaped tubes at different angles of attack

3.4 The turbulent kinetic energy

From Fig. 11, the turbulent kinetic energy increases across the tube banks for all the varying angles of attack. This is partly due to the effects of the preceding columns on the flow over the tubes downstream. The turbulence kinetic energy is maximum at regions close to the separation points on the tube walls across the columns and at regions behind the wakes generated by the tubes in the last column. Hence, regions characterized with higher turbulent kinetic energy are highly turbulent regions with higher heat transfer rates.
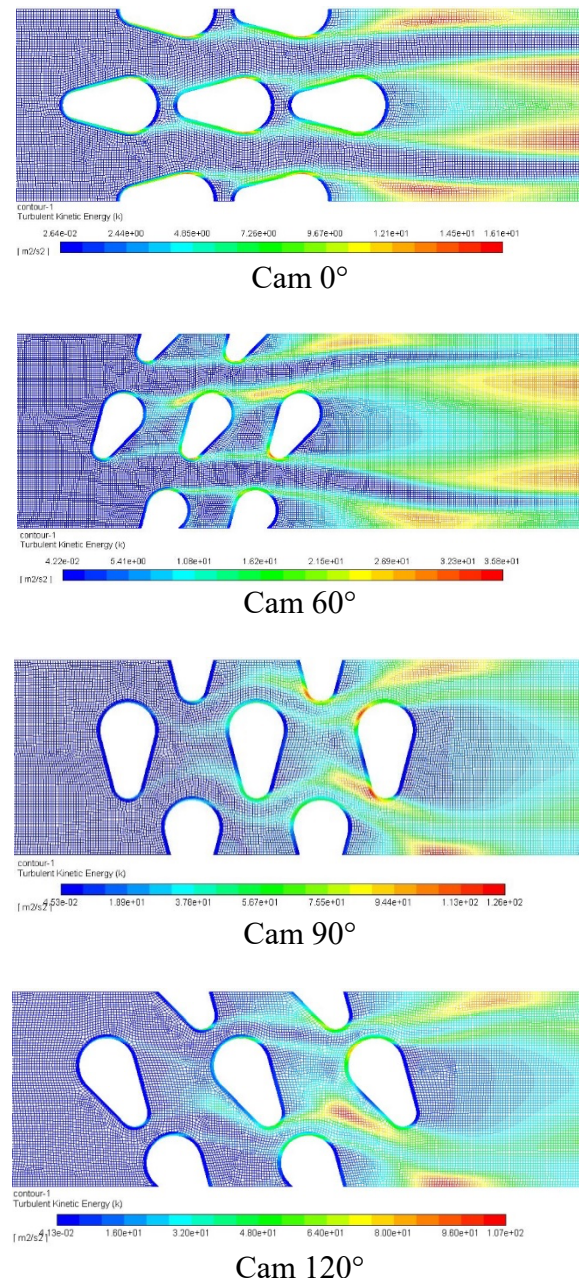

Fig. 11. Turbulent kinetic energy contour for the circular and cam-shaped tube banks at inlet velocity 9 m/s.

3.5 Effect of changing angle of attack on heat transfer performance

The effect of changing angle of attack of the cam-shaped tube bank on the Nusselt number is shown in Fig. 12. As it is clearly indicated, the Nusselt number increases with airflow velocity across both circular and cam-shaped tube banks at varying angles of attack. The values of the Nusselt numbers for flow over cam tube banks at angles of attack: 30°, 90° and 120° are 5.9, 33.9, and 32.1% higher over the range of Reynolds numbers than that circular tube bank, respectively. The cam tube bank at 0°, 60°, 150° and 180° exhibit lower Nusselt number with 26.1, 8.5, 23.5 and 25.4% difference as compared with the circular tube banks. The cam-shaped tubes at 90° and 120° exhibited greater Nusselt numbers partly due to the larger surface interaction in transverse flow and higher turbulent intensity within the tube banks than similar interaction of the flow with tube banks at 0° and 180°.
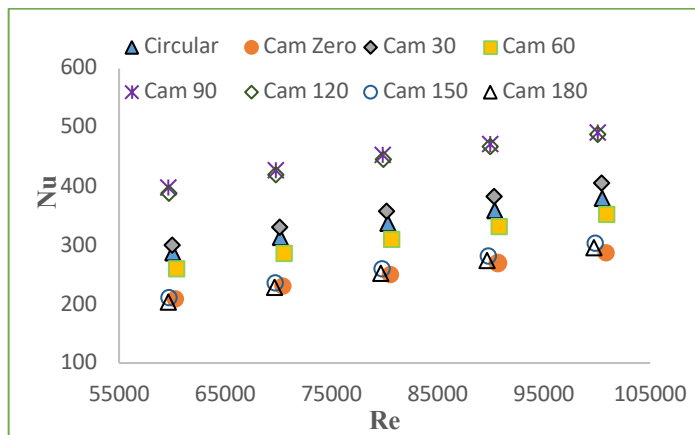
Fig. 12 Variation of the Nusselt number and Reynolds number of the tube banks.

3.6 Effect of changing angle of attack on thermal hydraulic performance

The thermal-hydraulic performance of the cam-shaped tubes in comparison with circular tubes over range of Reynolds numbers is as shown in Fig. 13. Clearly from the figure, the cam tubes at angles of attack 150° and 180° exhibited higher thermal hydraulic performance, higher than the circular tube bank by 167.6 and 284.3%, respectively while the cam-shaped tube bank at angle of attack 90° and 120° exhibited the minimum thermal hydraulic performance, lesser by 52.6 and 45.1%, respectively. Generally, cam-shaped tube banks performed better in terms of thermal hydraulic performance than circular tube banks, except for cam-shaped tube banks at 90° and 120° angles of attack. The lower thermal-hydraulic performance demonstrated by the tubes at 90° and 120° could be attributed to the high pressure drag caused from the orientation of the tubes to the flow direction.
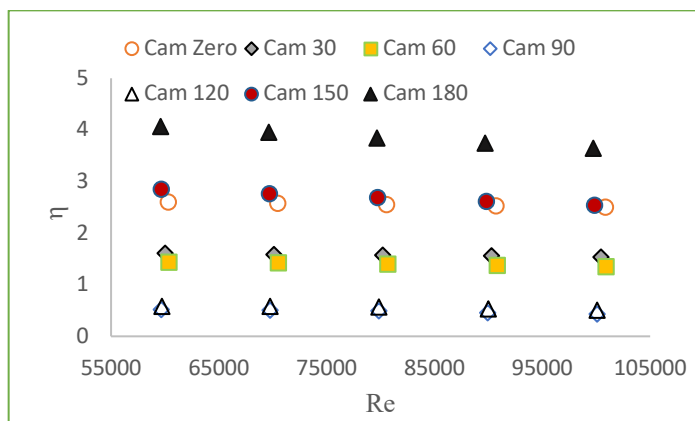

Fig. 13. The thermal-hydraulic performance of the cam-shaped tube banks

4. CONCLUSIONS

Circular tube banks and cam-shaped tube banks at angles of attack; 0°, 30°, 60°, 90° 120°, 150° and 180° were numerically and comparatively studied to examine their flow and heat transfer behaviour. The numerical analysis was performed to resolve the realizable k-ε turbulent model using ANSYS Fluent solver. The heat transfer and friction factor characteristics of the flow were the parameters primarily considered. The friction factor and Nusselt number of the cam-shaped tubes increased with increase in the air angle of attack from 0° to 90°, though with decrease in thermal-hydraulic performance. However, there were reductions in friction factor and Nusselt number when the angles were increase from 90° to 180° but with increase in the thermal-hydraulic

performance. Higher friction factor and Nusselt number were recorded when cam-shaped tubes were at angles of attack 90° and 120°. The cam-shaped tube bank at 180° angle of attack exhibited the maximum thermal-hydraulic performance. Thus, the cam-shaped tube banks at different angles attack provide enhanced heat transfer properties in relation to the circular tube bank. The changes in the angles of attack of the cam tubes caused improvement in thermal-hydraulic performance.

NOMENCLATURE

A	Surface area of a tube bank, m^2;
D_{eq}	Equivalent diameter; m;
f	Friction factor;
k	Turbulence kinetic energy, m^2/s^2;
N	Number of main resistance;
Nu	Nusselt Number;
Pr_T	Turbulent Prandtl number;
Q	Heat transfer rate, W;
Re	Reynolds number;
S_L	Longitudinal pitch, m;
S_T	Transverse pitch, m;

Greek symbols

Δp	Pressure drop, Pa;
ε	Dissipation rate, m^2/s.
η	Thermal hydraulic performance factor.
γ	Thermal conductivity, W/(m.K)
ρ	Density, kg/m^3;
μ	Dynamic viscosity, Pa.s;
μ_T	Turbulent eddy viscosity, Pa.s;

REFERENCES

Abolfathi, S., Mirabdolah Lavasani, A., Mobedi, P., and Salehi Afshar, K. 2021, "Experimental study on flow around a tube in mixed tube bundles comprising cam-shaped and circular cylinders in in-line arrangement," *International Journal of Thermal Sciences*, *163*, 106812. https://doi.org/10.1016/j.ijthermalsci.2020.106812

Ahmed, M. A., Yaseen, M. M., and Yusoff, M. Z. 2017, "Numerical study of convective heat transfer from tube bank in cross flow using nano fluid," *Case Studies in Thermal Engineering*, *10*, 560–569. https://doi.org/10.1016/j.csite.2017.11.002

Alnakeeb, M. A., Saad, M. A., and Hassab, M. A. 2021, "Numerical investigation of thermal and hydraulic performance of fin and flat tube heat exchanger with various aspect ratios," *Alexandria Engineering Journal*, *60*(5), 4255–4265. https://doi.org/10.1016/j.aej.2021.03.036

Bahaidarah, H. M. S., Anand, N. K., and Chen, H. C. 2005, "*A numerical study of fluid flow and heat transfer over a bank of flat tubes," December 2004*, 359–385. https://doi.org/10.1080/10407780590957134

Bayat, H., Lavasani, A. M., and Maarefdoost, T. 2014, "Experimental study of thermal-hydraulic performance of cam-shaped tube bundle with staggered arrangement," *Energy Conversion and Management*, *85*, 470–476. https://doi.org/10.1016/j.enconman.2014.06.009

Bergman, T. L., Lavine, A. S., Incropera, F. P., and Dewitt, D. P. 2011, *Fundamentals of heat and mass transfer,* (7th ed.). John Wiley and Sons.

Deeb, R. 2021, "Experimental and numerical investigation of the effect of angle of attack on air flow characteristics around drop-shaped tube." *Physics of Fluids*, *33*(6), 065110. https://doi.org/10.1063/5.0053040

Deeb, R. 2022, "Numerical analysis of the effect of longitudinal and transverse pitch ratio on the flow and heat transfer of staggered drop-shaped tubes bundle," *International Journal of Heat and Mass Transfer*, *183*, 122123. https://doi.org/10.1016/j.ijheatmasstransfer.2021.122123

Ge, Y., Lin, Y., Tao, S., He, Q., Chen, B., and Huang, S. M. 2021, "Shape optimization for a tube bank based on the numerical simulation and multi-objective genetic algorithm," *International Journal of Thermal Sciences*, *161*, 106787. https://doi.org/10.1016/j.ijthermalsci.2020.106787

Guan-min, Z., Xue-li, L., Nai-xiang, Z., and Yan-ping, S. H. I. 2015, "Flow and heat transfer characteristics around egg-shaped tube," *Journal of Hydrodynamics*, *27*(1), 76–84. https://doi.org/10.1016/S1001-6058(15)60458-9

Han, H., He, Y., Li, Y., Wang, Y., and Wu, M. 2013, "International Journal of Heat and Mass Transfer A numerical study on compact enhanced fin-and-tube heat exchangers with oval and circular tube configurations," *International Journal of Heat and Mass Transfer*, *65*, 686–695. https://doi.org/10.1016/j.ijheatmasstransfer.2013.06.049

Holman, J. P. 2010, *Heat Transfer* (10th ed.). McGraw-Hill.

Huang, J., and Jang, J. 2012, "Numerical Investigation of Nanofluids Laminar Convective Heat Transfer through Staggered and In-Lined Tube Banks," In F. L. Gaol et al. (Ed.), *2nd International Congress on CACS, AISB 144* (pp. 483–490). Springer-Verlag.

Khan, W. A., Culham, J. R., and Yovanovich, M. M. 2006, "Convection heat transfer from tube banks in crossflow: Analytical approach," *International Journal of Heat and Mass Transfer*, *49*, 4831–4838. https://doi.org/10.1016/j.ijheatmasstransfer.2006.05.042

Khurmi, R. S., & Gupta, J. K. 2005, *Theory of Machines* (14th ed.). S. Chand and Co. Ltd.

Lavasani, A. M. 2011, "The Effect of Angle of Attack on Pressure Drag from a Cam Shaped Tube," *International Journal of Mechanical, Aerospace, Industrial, Mechatronic and Manufacturing Engineering*, *5*(1), 28–32.

Lavasani, A. M., and Bayat, H. 2016, "Numerical study of pressure drop and heat transfer from circular and cam-shaped tube bank in cross-flow of nanofluid," *Energy Conversion and Management*, *129*, 319–328. https://doi.org/10.1016/j.enconman.2016.10.029

Lavasani, A. M., Bayat, H., and Maarefdoost, T. 2014, "Experimental study of convective heat transfer from in-line cam shaped tube bank in crossflow," *Applied Thermal Engineering*, *65*, 85–93. https://doi.org/10.1016/j.applthermaleng.2013.12.078

Mangrulkar, C. K., Dhoble, A. S., Chamoli, S., Gupta, A., and Gawande, V. B. 2019, "Recent advancement in heat transfer and fluid flow characteristics in cross flow heat exchangers," *Renewable and Sustainable Energy Reviews*, *113*(109220), 1–31. https://doi.org/10.1016/j.rser.2019.06.027

Mangrulkar, C. K., Dhoble, A. S., Deshmukh, A. R., and Mandavgane, S. A. 2016, "Numerical investigation of heat transfer and friction factor characteristics from in-line cam shaped tube bank in crossflow," *Applied Thermal Engineering*, *110*, 521–538. https://doi.org/10.1016/j.applthermaleng.2016.08.174

Mangrulkar, C. K., Dhoble, A. S., Sathe, T. M., Chamoli, S., and Arunkumar, H. S. 2018, "Thermal performance intensification of cam shaped tubes in staggered layout," *International Conference on Computational Methods for Thermal Problems*, *223309*, 211–214.

Nada, S. A., El-Batsh, H., and Moawed, M. 2007, "Heat transfer and fluid flow around semi-circular tube in cross flow at different orientations," *Heat and Mass Transfer*, *43*(11), 1157–1169. https://doi.org/10.1007/s00231-006-0202-y

Nouri-Borujerdi, A., and Lavasani, A. M. 2007, "Experimental study of forced convection heat transfer from a cam shaped tube in cross flows," *International Journal of Heat and Mass Transfer*, *50*, 2605–2611. https://doi.org/10.1016/j.ijheatmasstransfer.2006.11.028

Nouri-Borujerdi, A., and Lavasani, A. M. 2008, "Pressure Loss and Heat Transfer Characterization of a Cam-Shaped Cylinder at Different Orientations," *Journal of Heat Transfer*, *130*(124503), 1–4. https://doi.org/10.1115/1.2969259

Petinrin, M. O., Towoju, O. A., Ajiboye, S. A., and Zebulun, O. E. 2019, "Numerical study of the effect of changing tube pitches on heat and flow characteristics from tube bundles in cross flow," *Journal of Engineering Sciences*, *6*(2), 1–10. https://doi.org/10.21272/jes.2019.6(2).e1

Shih, T. H., Liou, W. W., Shabbir, A., Yang, Z., and Zhu, J. 1995, "A new k-e eddy viscosity model for high reynolds number turbulent flows - model development and validation," *NASA Technical Memorandum*, *24*(3), 227–238.

Toolthaisong, S., and Kasayapanand, N. 2015, "Heat Transfer Enhancement in a Cross-Flow Heat Exchanger with Modified Air Angles of Attack," *Journal of Energy Engineering*, *04015044*, 1–6. https://doi.org/10.1061/(ASCE)EY.1943-7897.0000316.

Xiao, C., and Zhang, G. 2022, "Arrangement Effect on Heat Transfer and Hydrodynamic Characteristics of a Tube Bank in Cross Flow," *Computational Thermal Sciences: An International Journal*, *14*(6).